

Electronic Supplementary Information

Unconventional two-dimensional germanium dichalcogenides

Jiang-Jing Wang, Ider Ronneberger, Ling Zhou, Lu Lu, Volker L. Deringer, Baiyu Zhang, Lin Tian, Hongchu Du, Chunlin Jia, Xiaofeng Qian, Matthias Wuttig, Riccardo Mazzarello, and Wei Zhang*

The recently discovered two-dimensional (2D) group IV chalcogenides attract a lot of attention owing to their novel electronic and photonic properties. All reported materials of this class favor (distorted) octahedral coordination via p bonding; by contrast, in the dichalcogenides where the bonding tendency approaches sp^3 , no corresponding 2D phase has been realized so far. Here, by engineering the composition of a chalcogenide heterostructure, the hitherto elusive GeTe₂ is experimentally observed in a confined 2D environment. This new structural motif exhibits octahedral coordination and can withstand high tensile strain (~10%). Density functional theory simulations predict the existence of freestanding monolayer GeTe₂ under tensile strain, and the existence of GeSe₂ and GeS₂ in the same form at equilibrium conditions. The newly found 2D germanium dichalcogenides display either metallic or narrow gap semiconducting behaviors, and may lead to new applications in nanoscale electronics.

Methods

Sample preparation: The ~80 nm Te-rich GeSbTe films were deposited with the magnetron sputtering technique on ultra-thin carbon film (3~5nm) TEM grids. The GeSbTe films were covered by a thin ZnS-SiO₂ layer to prevent oxidation. The capping layer is electron-transparent. The samples were annealed in argon atmosphere (flow rate of 200 sccm) in a regular tube furnace with a 1 cm diameter quartz tube. The annealing procedure started from room temperature to 300 °C, the heating rate was 5 K/min and the holding time at the anneal temperature was 1 hour. After this period, the sample was naturally cooled to near room temperature, and then removed from the furnace.

TEM experiments: Atomic-resolution high-angle annular dark field (HAADF) imaging experiments were performed on a JEOL ARM200F scanning transmission electron microscope with a probe aberration corrector, operated at 200 kV. In the STEM mode, a probe size of 0.1 nm and convergence angle of 22 mrad were used for HAADF imaging experiments. The HAADF detectors covered an angular range of 68 to 280 mrad. Electron energy loss spectroscopy (EELS) and energy-dispersive X-ray spectroscopy (EDS) experiments were carried out on a JEM2100F microscope at 200 kV.

DFT simulations: Simulations were carried out using two codes, the Vienna Ab initio Simulation Package (VASP)^[1] and the Quantum Espresso (QE) package.^[2] The electronic structure calculations and projected Crystal Orbital Hamiltonian Population (COHP)^[3-5] analyses were done by using VASP and processing the self-consistent wavefunctions using LOBSTER,^[6] while the phonon simulations were done by using QE under the density functional perturbation theory scheme.^[7] For both sets of simulations, generalized gradient approximated (GGA) functionals^[8] were used and augmented with van der Waals corrections.^[9] Dense Monkhorst-Pack (MP) k-point meshes^[10] from 30×30×1 up to 60×60×1 were used. Projector augmented-wave pseudopotentials and ultrasoft pseudopotentials were used in VASP and QE simulations, respectively. The employed energy cutoff of plane waves is 500 eV for VASP and 65 Ryd for QE. Both the volume and atomic positions of monolayer GeX₂ (X = S, Se and Te) were fully relaxed. The HSE06 hybrid functional^[11] was employed to crosscheck the band structure calculations, and the results are very close to the GGA calculations. In general, HSE06 leads to a small reduction for the gap size ~0.05 eV for all the semiconducting models, but does not affect the overall shape of the band structures. The above simulations were done by employing unit cell models. 3×3×1 supercell models were constructed and relaxed, and no difference in structural properties was observed.

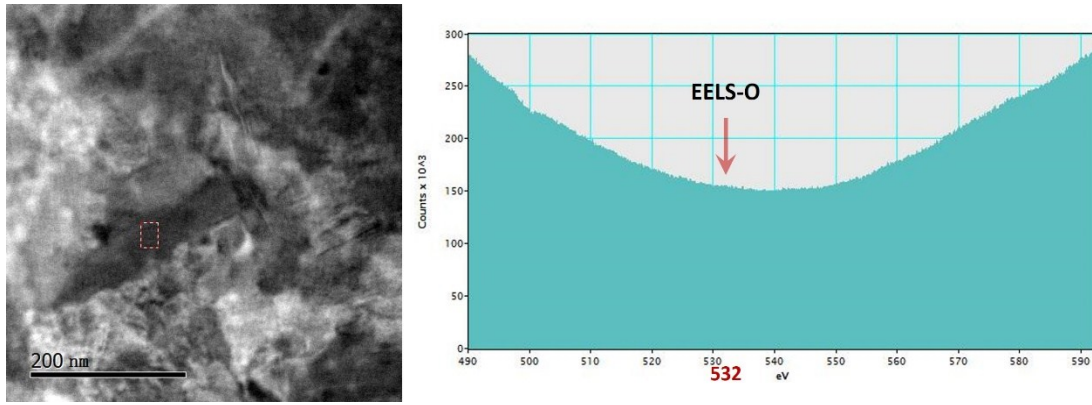


Figure S1. TEM image and electron energy loss spectroscopy (EELS) spectrum of hexagonal GeSbTe sample. The EELS spectrum was obtained in the boxed region shown on the TEM image. Clearly, no oxygen peak is detected in the spectrum.

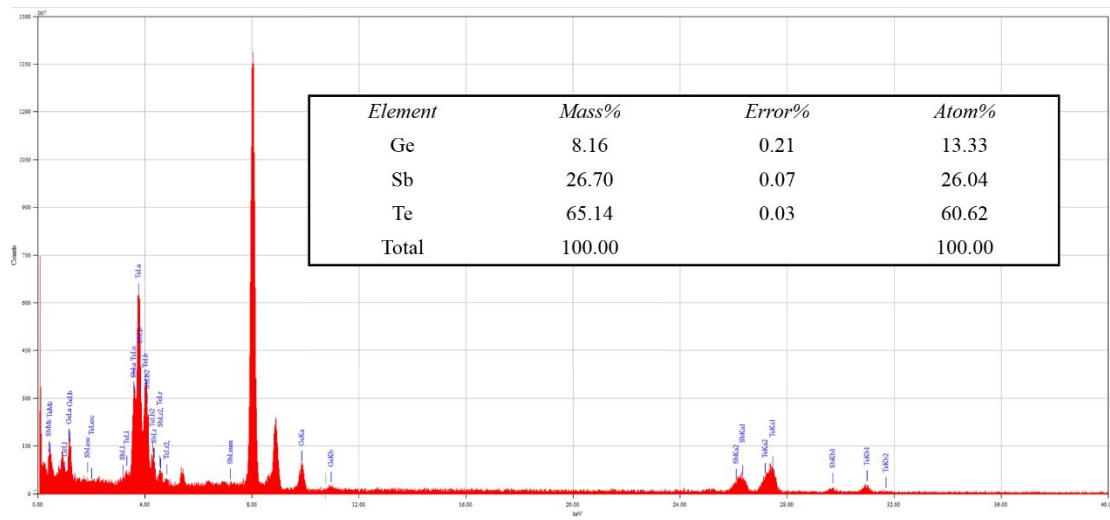


Figure S2. Energy-dispersive X-ray spectroscopy (EDS) measurements of a GeSbTe grain. The stoichiometry is close to $\text{Ge}_{1.02}\text{Sb}_2\text{Te}_{4.66}$. Although this technique is semi-quantitative, it indicates an excess of Te in our sample.

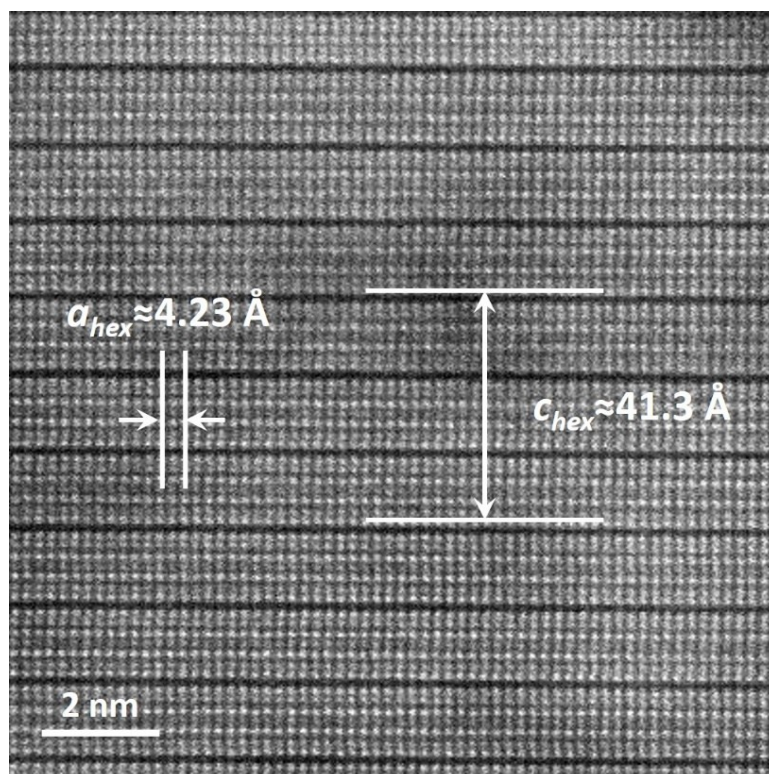


Figure S3. STEM-HAADF image of the Te-rich sample along the $[01\bar{1}0]$ direction. The measured lattice parameters of GeSb_2Te_4 blocks are $a_{\text{hex}} \approx 4.23 \text{ \AA}$ and $c_{\text{hex}} \approx 41.3 \text{ \AA}$.

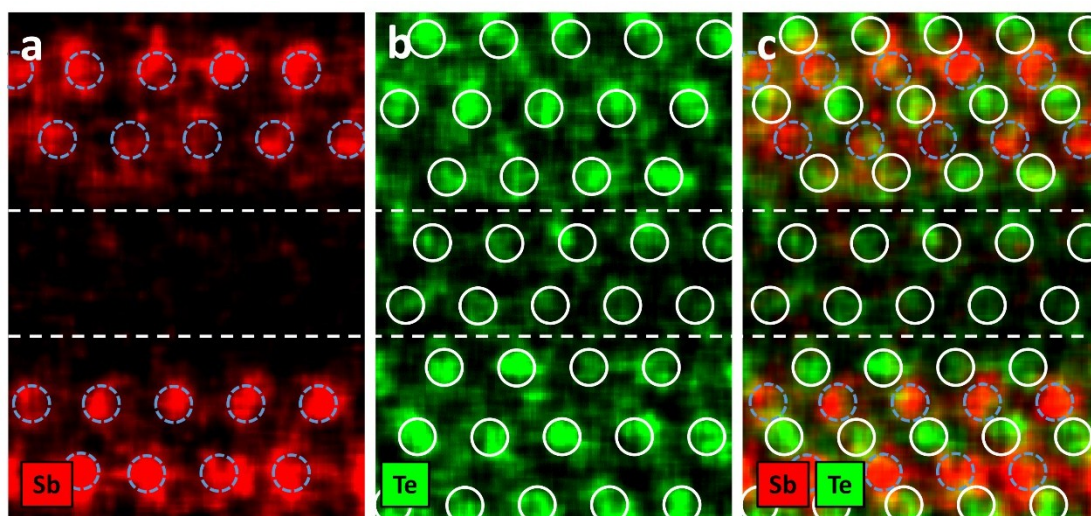


Figure S4. EDS mapping. a-c are Sb (red), Te (green) and mixed EDS mapping, respectively. The positions of the Sb and Te atoms are marked with dashed circles and solid circles, respectively. The signal of Ge is too weak to be detected in this EDS mapping experiment, owing to its low atomic number and dechanneling effects. Nevertheless, EDS mapping clearly shows that there is no Sb contribution from the triple-layer structure, which rules out the possibility of Sb+vacancy combination.

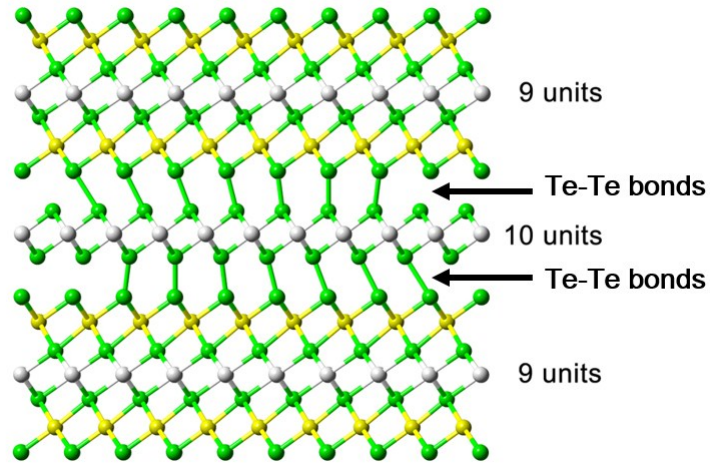


Figure S5. Strong lattice mismatch between 2D GeTe_2 with calculated lattice parameter and GeSb_2Te_4 blocks with the experimental bulk value. The very high amount of unfavorable Te-Te covalent bonds generates high in-plane tensile strain to 2D GeTe_2 .

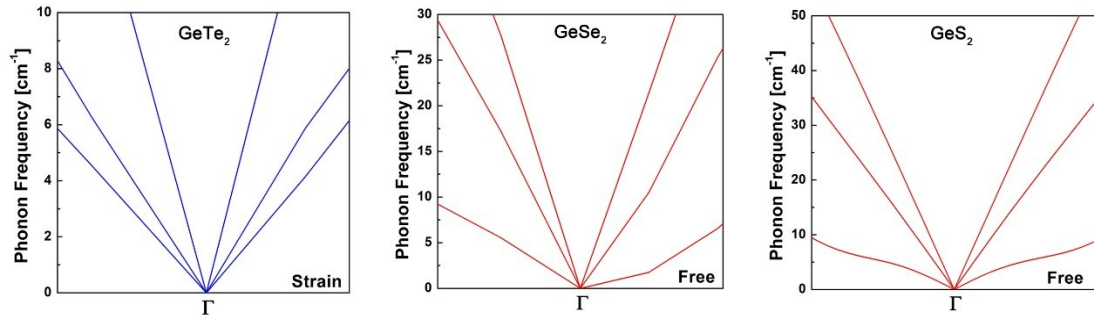


Figure S6. The zoomed-in views of phonon dispersion curves of strained 2D GeTe_2 and freestanding 2D GeSe_2 and GeS_2 . The absence of imaginary frequencies suggest these three models to be dynamically stable.

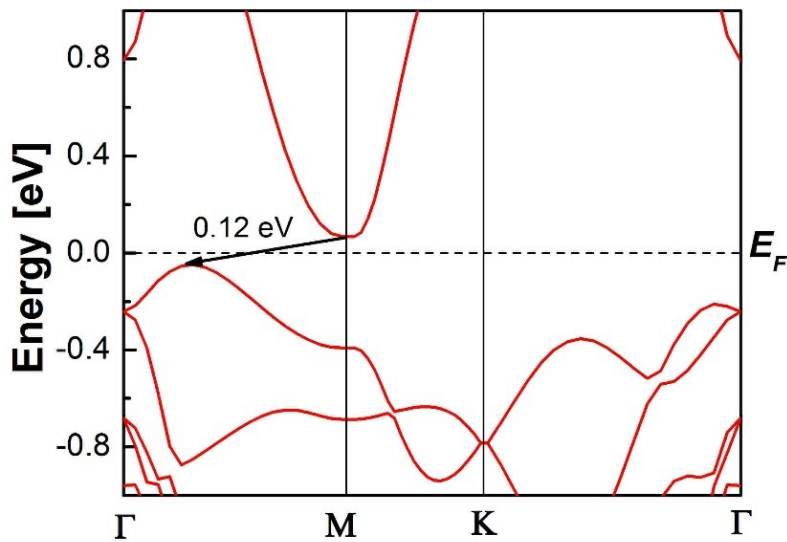


Figure S7. A zoom-in view of the band structure of 2D GeSe_2 at 4% tensile strain. The band gap is indirect, and the gap size is ~ 0.12 eV. The minimum of conduction band is located at M point, while the top of the valence band is found in the middle of the $\Gamma \rightarrow \text{M}$ path.

References

- [1] G. Kresse, F. J., *Phys. Rev. B* 1996, **54**, 11169.
- [2] P. Giannozzi, S. Baroni, N. Bonini, M. Calandra, R. Car, C. Cavazzoni, D. Ceresoli, G. L. Chiarotti, M. Cococcioni, I. Dabo, A. Dal Corso, S. de Gironcoli, S. Fabris, G. Fratesi, R. Gebauer, U. Gerstmann, C. Gougoussis, A. Kokalj, M. Lazzeri, L. Martin-Samos, N. Marzari, F. Mauri, R. Mazzarello, S. Paolini, A. Pasquarello, L. Paulatto, C. Sbraccia, S. Scandolo, G. Sclauzero, A. P. Seitsonen, A. Smogunov, P. Umari, R. M. Wentzcovitch, *J. Phys. Cond. Matt.* 2009, **21**, 395502.
- [3] R. Dronskowski, P. E. Blöchl, *J. Phys. Chem.* 1993, **97**, 8617.
- [4] V. L. Deringer, A. L. Tchougreff, R. Dronskowski, *J. Phys. Chem. A* 2011, **115**, 5461.
- [5] S. Maintz, V. L. Deringer, A. L. Tchougréeff, R. Dronskowski, *J. Comput. Chem.* 2013, **34**, 2557.
- [6] S. Maintz, V. L. Deringer, A. L. Tchougreff, R. Dronskowski, *J. Comput. Chem.* 2016, **37**, 1030.
- [7] S. Baroni, S. de Gironcoli, A. Dal Corso, P. Giannozzi, *Rev. Mod. Phys.* 2001, **73**, 515.
- [8] J. P. Perdew, K. Burke, M. Ernzerhof, *Phys. Rev. Lett.* 1996, **77**, 3865.
- [9] S. Grimme, *J. Comput. Chem.* 2006, **27**, 1787.
- [10] H. J. Monkhorst, J. D. Pack, *Phys. Rev. B* 1976, **13**, 5188.
- [11] J. Heyd, G. E. Scuseria, M. Ernzerhof, *J. Chem. Phys.* 2003, **118**, 8207.